International Research Journal of Engineering and Technology (IRJET) e-ISSN: 2395-0056
Volume: 05 Issue: 05 | May-2018 www.irjet.net p-ISSN: 2395-0072

Fabrication and Analysis of NACA 0012 Airfoil in Wind Tunnel

Mohit Singh

P. G. Student, Department of Mechanical Engineering, CBS group of Institutions, Jhajjar, MDU, Haryana, India

---

Abstract - *The major aerodynamic principles being focused on during this project include that a symmetric airfoil does not generate lift at a zero angle of attack. Since NACA 0012 is symmetric about its chord line i.e. at zero angle of attack there is no lift. Another fundamental principle is that lift is created over an airfoil by the pressure differences over the top and bottom surfaces of the airfoil. Drag over an airfoil is caused by drag due to lift (induced drag), skin friction, as well as pressure. The drag due to lift is caused by the tip vortices of the airfoil not extending to the walls of the wind tunnel and allowing the high pressure to interact with the relative low pressures along the top surface of the airfoil causing a loss in lift. The drag due to skin friction is due to the molecules passing over the surface of the airfoil and some sticking to the surface in the no slip condition. The pressure drag is created by the stagnation point in the front of an airfoil which impedes the flow of the fluid over the airfoil. This whole analysis is done at subsonic flow.*

I. INTRODUCTION

When a body moves through a fluid or fluid moves over the surface of the body then there is formation of boundary layer. Existence of boundary layer leads to the various forces acting on the body. These forces are Normal force, Axial force, Drag force, Lift force. If body is having aerodynamic shape, then the generated lift force will help to lift, up or down the body in the fluid depending on the angle at which the air is striking the body. The NACA airfoils are airfoil shapes for aircraft wings developed by the National Advisory Committee for Aeronautics (NACA). The shape of the NACA airfoils is described using a series of digits following the word "NACA". The parameters in the numerical code can be entered equations to precisely generate the cross-section of the airfoil and calculate its properties.

Important terms-In the aerodynamic design of airfoil some common terms are given below

A. Leading Edge - Point at the front of the airfoil which has the maximum curvature and flowing fluid strikes the surface firstly at this point.

B. Trailing Edge - The point of maximum curvature at the rear end of airfoil.

C. Chord Line - Straight line joining the leading edge and trailing edge is called as chord length

D. Chord Length - Simply CHORD, is the length of the chord line and is the characteristic dimension of the airfoil section.

E. Camber Line - A line on a cross section of a wing of an aircraft which is equidistant from the upper and lower surfaces of the wing.

F. Angle of Attack - In fluid dynamics, angle of attack (AOA), or α[1] is the angle between a reference line on a body (often the chord line of an airfoil) and the vector representing the relative motion between the body and the fluid through which it is moving. Angle of attack is the angle between the body's reference line and the oncoming flow. In aerodynamics, angle of attack specifies the angle between the chord line of the wing of a fixed-wing aircraft and the vector representing the relative motion between the aircraft and the atmosphere. Since a wing can have twist, a chord line of the whole wing may not be definable, so an alternate reference line is simply defined. Often, the chord line of the root of the wing is chosen as the reference line. Another choice is to use a horizontal line as the reference line.

For the symmetrical airfoil there is no camber present which means that chord line and camber line are same.
Based on numerical digits, it is mainly classified into two parts which are given below

1. Four-digit Series - The NACA four-digit wing sections define the profile by:

First digit describing maximum camber as percentage of the chord.

Second digit describing the distance of maximum camber from the airfoil leading edge in tens of percent of the chord.

Last two digits describing maximum thickness of the airfoil as percent of the chord.

NACA 0012 mean that there is no camber i.e. zero camber is present, and it has the maximum thickness of the airfoil at 12% of the chord from the leading edge.

2. Five-digit Series - The NACA five-digit series describes more complex airfoil shapes

The first digit, when multiplied by 0.15, gives the designed coefficient of lift (C_l).

Second and third digits, when divided by 2, give the location of maximum camber as a distance from the leading edge (as per cent of chord).

Fourth and fifth digits give the maximum thickness of the airfoil (as per cent of the chord).

For example, the NACA 12018 airfoil would give an airfoil with maximum thickness of 18% chord, maximum camber located at 10% chord, with a design lift coefficient of 0.2.

II. EXPERIMENTAL SETUP

Wind Tunnel[8] - Wind-tunnels represent a useful tool for investigating various flow phenomena. An advantage of using wind-tunnels is that experiments there can be performed under well controlled circumstances compared to experiments in the open environment.

There are many types of wind-tunnels and they can be classified according to the flow speed into four categories.

1. Subsonic or low-speed wind-tunnels
2. Transonic wind-tunnels
3. Supersonic wind-tunnels
4. Hypersonic wind-tunnels

In the present work, a low speed subsonic wind tunnel has been used. Cross section of the test chamber is 300*300mm^2 area of the inlet section is 850*850mm^2, so the contraction ratio is 8.03. Area of the diffuser part is660*660mm^2 with axial exhaust fan of 1300 rotation per minute(rpm). To measure the velocity of air in the tunnel we have used pitot tube.

Wind tunnel used for the experiment is shown in the figure below

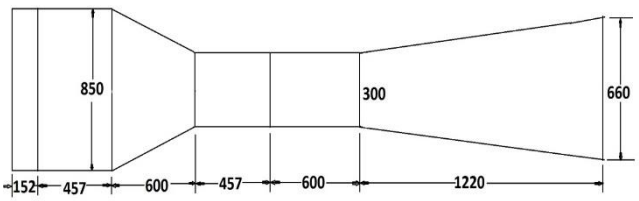

Fig. II-a Wind tunnel

Air is sucked through a duct equipped with a viewing port and instrumentation where models or geometrical shapes are mounted for study. Typically, the air is moved through the tunnel using a series of fans. For very large wind tunnels several meters in diameter, a single large fan is not practical, and so instead an array of multiple fans is used in parallel to provide sufficient airflow.

In our present work wind tunnel was subsonic so there was only one axial electric fan was used.
The airflow created by the fan that is entering the tunnel is itself highly turbulent due to the fan blade motion (when the fan is blowing air into the test section, when it is sucking air out of the test section downstream), and so is not directly useful for accurate measurements. The air moving through the tunnel needs to be relatively turbulence-free and laminar. To correct this problem, closely spaced PVC pipes was used after these pipe section a very small size of mesh was used to smooth out the turbulent airflow before reaching the subject of the testing.

Model--The model used for the experiment was standard NACA0012 airfoil. NACA0012 airfoil is a symmetrical low lift airfoil with maximum thickness being 12% of the chord located at 30% of the chord length.
The airfoil shape is shown in figure. The points indicate the location of pressure ports.

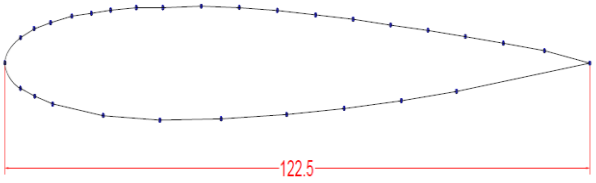

Fig. II-b NACA 0012 with pressure ports

Model Fabrication and Pressure Porting - The model was fabricated by acrylic. Aerodynamic contour of the airfoil was obtained by the CNC machine. It has three parts; the center part has the pressure ports of 0.8mm diameter on both upper and lower surfaces which were drilled by the CNC machine. The total no of pressure ports was 29 in which 15 ports are at the upper surface and 12 ports are on the lower surface remaining two ports are at the leading and trailing edge. Surface pressure ports are more clouded around the leading edge so that we can get more pressure accurate distribution. Through hole are made at the front face up to the half span length of airfoil, having diameter of 1.22 mm to connect the pressure ports from manometer by the help steel tube of diameter of 1.2 mm. These steel tubes are further connected by rubber tube to connect to the manometer.

Since the model was fabricated into three parts so these parts are assembled to each other by the help of chloroform which reacts with acrylic sheet and sticks to each other.

Final model has some small irregularities on the surface, to remove these irregularities very fine sand paper of grit size P400 is used.

Model Mounting--The model was taken inside the test section of the wind tunnel and was rigidly mounted end-to-end with ball bearings on the glass side and a iron piece fixed on the other side which provides the facility to rotate and fix the model by the help of volt. To mount the model on the left and right face two hole of 8mm diameter is provided in which steel rod was inserted, these steel rods are inserted into bearing which is fixed into the test chamber. To measure the angle of attack of wind at the airfoil a protector was provided, to fix the model at an angle of attack. Angle of model was controlled by loosening the screw, fixing the model at the required angle and then tightening the screw.

Pressure Measurement--Pressure measurement was done by the manometer, which was made by the combination of glass tube with the PVC pipe. PVC pipe was connected by the reservoir which maintain the petrol requirement for the manometer glass tube. Working fluid used in the manometer was petrol because of its lower density compared to water.

Glass tubes are connected to the model by the help of plastic pipes and steel tube.
Manometer assembly was fixed at the plywood, axis of the plywood was 30˚ inclined to the vertical axis to increase the sensitivity of the manometer i.e. by inclining the manometer for the same pressure head we get the more rise in the glass tube column.

When air was sucked by the fan it creates the pressure distribution along the surface of the airfoil. Pressure ports provided at the surface of airfoil was connected to the connected to manometer by the steel tubes and plastic pipes. Generation of pressure distribution ay the surface will generate the pressure difference along the manometer which lifts the petrol level in the glass tube. Rise of the petrol level in each glass tube will depend upon the pressure difference created across the corresponding pressure port.

When the angle of attack ranging from -12˚ to +14˚ there was large difference of petrol level in the glass tube, but after this range of angle all the liquid column of manometer shows almost same reading which shows the stalling behavior of the airfoil.

III. DATA ACQUISTION AND ANALYSIS

In the data acquisition process first step was to note down the pressure variation in the excel sheet corresponding to the pressure port profile. Port map file which contain the location of every ports w.r.t. the chord length(c) was obtained by the Creo software in which designing of the model pressure porting was done. This Creo file was used to manufacture the model. By measuring the x and y co-ordinate of each port by the help of software each measurement was divided by the chord length(c) of the model. Port map file was used in the calculation forces acting on the model to get the characteristics of the model.

The objective of present experiment was to investigate the effect of angle of attack and Reynolds number on the airfoil characteristics. To do this experiment four set of tests were done. Each test was done at number. Each set of tests was done at different angle of attack, variation of angle of attack is from the -14 to +15 degrees in the increment of 2 degree. To verify the reading each set of tests was repeated at an angle in the last of every set experiment.

Each set of tests was done after the sometime interval to get the accurate result, because if the test is continued is for long time then due to heat generated by the friction forces present in the wind tunnel rises the temperature of air which causes the decrease in the density of air because of which results will not be accurate.

Details of each set is given below

A. First set of experiment was done at the velocity of 9.82 m/s variation of angle of attack was from the -14˚ to +15˚ in the interval of 2˚, the repeatability test was done at the angle of attack 6˚.

B. Second set of experiment was done at the velocity of 8.5m/s and repeatability test were done at the angle of attack at 8˚.

C. Third set of experiment was done at the velocity of 7.76 m/s and repeatability test was done at the angle of attack at the 6˚.

D. Fourth set of tests was done at the velocity of 6.94 m/s and repeatability test was done at the 8˚.

Data Analysis - The raw data which was stored in the excel sheet at the time of data acquisition was used to calculate the different characteristic of the model.

In the data analysis program first thing was to calculate the value of coefficient of pressure (C_p) for each pressure port.

Calculation of lift coefficient (C_l)[1] -- Firstly, the pressure data was converted into non-dimensional form called coefficient of pressure C_p[1] by subtracting free stream static pressure from the local pressure on the model, then dividing the result by dynamic head of the freestream. Then the pressure forces are integrated to get the force components along and perpendicular to airfoil chord; then the lift force is calculated by taking components of forces in direction perpendicular to freestream wind.

$$C_p = \frac{p_{local} - p_{static}}{\frac{1}{2}\rho U_\infty^2} = \frac{p_{local} - p_{static}}{p_{total} - p_{static}}$$

For an airfoil subjected to freestream wind velocity V_∞ at angle of attack α,

$$C_n = -\oint C_p \; d\left(\frac{x}{c}\right) \approx -\sum C_p \; \Delta x/c$$

$$C_a = \oint C_p \, d\left(\frac{y}{c}\right) \approx \sum C_p \; \Delta y/c$$

$$C_l = C_n \cos\alpha - C_a \sin\alpha$$

In fluid dynamics drag (sometimes called air resistance a type of friction, or fluid resistance, another type of friction) refers to forces acting opposite to the relative motion of any object moving with respect to a surrounding fluid. This can exist between two fluid layers (or surfaces) or a fluid and a solid surface. Unlike other resistive forces, such as dry friction, which are nearly independent of velocity, drag forces depend on velocity. Drag forces always decrease fluid velocity relative to the solid object in the fluid's path.

$$C_d = C_n \sin\alpha + C_a \cos\alpha$$

IV. RESULT AND DISCUSSION

The pre-requisite for any analysis of the experimental results is the validation of the experimental procedure/setup used for measurements. The preliminary surface pressure measurement data and the corresponding aerodynamic coefficients are firstly compared with existing literature for the NACA 0012 airfoil.

C_p variation - As mentioned above coefficient of pressure was calculated by the raw data collected at the time of experiment. These C_p values are plotted against the x/c at an angle of attack.

Variation of C_p with x/c at velocity of 9.81m/s is shown in figure given below

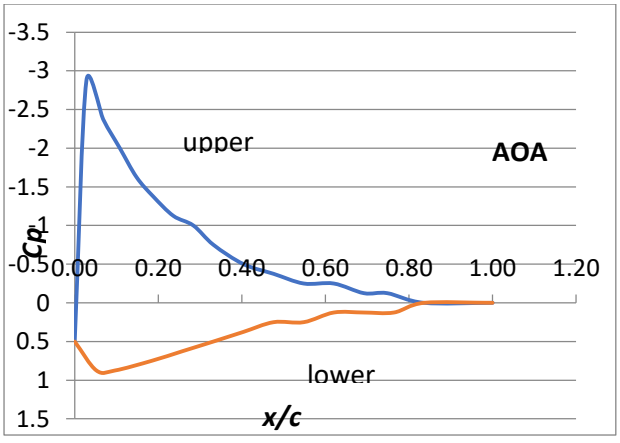

Fig. IV-a variation of *Cp* vs *x/c* graph

As the graph shows, value of *Cp* the leading edge is having the positive value and after that it has negative value for the upper surface and for the lower surface it has positive value throughout the surface which means that pressure distribution across the upper surface is lower than the lower surface, because of the pressure difference between the upper and lower surface airfoil will face the lift force. At the trailing edge *Cp* is having zero value which shows that pressure is the same as the free stream pressure.

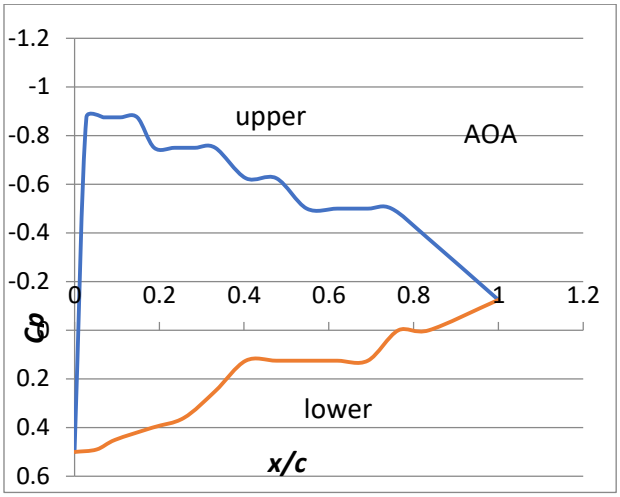

Fig. IV-b *Cp* vs *x/c*

Variation of *Cp* at the angle of attack 15° is shown in the above graph as the earlier discussion airfoil will start facing the stalling effect after +14° graph shows that there is almost no or very small pressure variation along the surface of the airfoil. In the stall condition large drag force will act on the airfoil with very small lift force.

Variation of lift coefficient with angle of attack at Reynolds number-- The lift curves were obtained at varying speeds from (6.94m/s to 9.82m/s) study the effect of Reynolds number on $C_{l\,\max}$ and stall angle. The plots of lift coefficient as a function of angle of attack at different Reynolds number are shown in Fig. IV-c.

It can be seen from fig. IV-d, that the plots are almost linear for smaller angles, and start deviating for larger angles (more than 7^0), even more so at larger Reynolds number. With increase in angle of attack, the flow, being unable to overcome the high adverse pressure gradients, starts separating from the trailing edge. As the incoming Reynolds number of the flow increases, the freestream turbulence is higher, due to which the boundary layer is having more turbulent kinetic energy, so it remains attached to the surface for longer distance compared to the case at lower Reynolds number. Due to this trailing edge flow separation, the lift coefficient is slightly lower at smaller value of Reynolds number at high angles of attack. It is also found that stall angle and hence $C_{l\,max}$ increases with Reynolds number. The turbulent boundary layer, having more energy tends to remain

attached to airfoil surface, and hence the airfoil stalls at a higher angle of attack at higher Reynolds number.

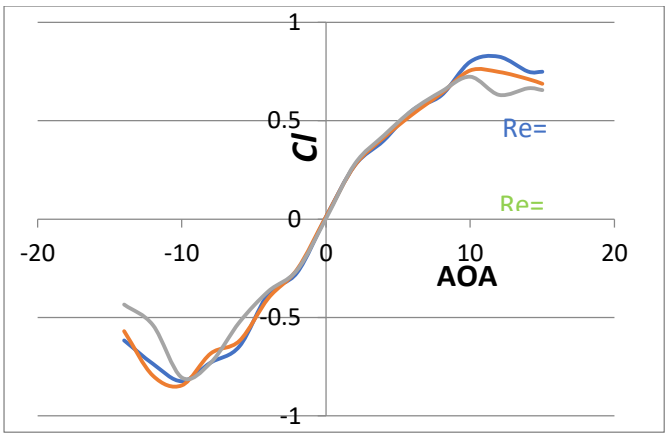

Fig. IV-c C_l versus α plot at different Reynolds numbers

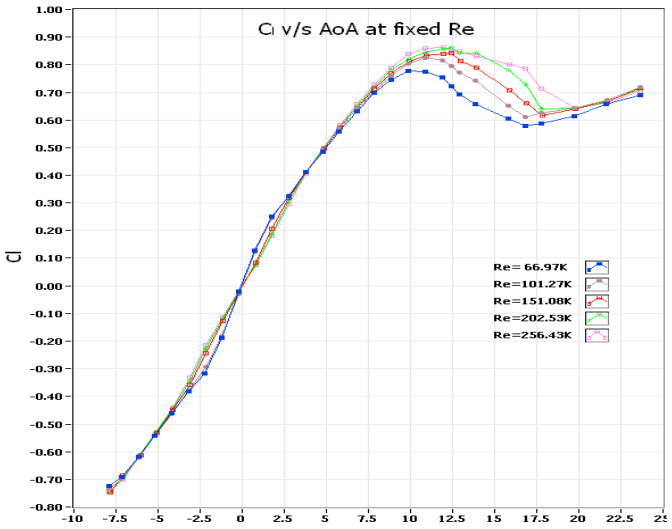

Fig. IV-d Reference Data [2]

The variation of the lift coefficient at a fixed angle of attack with the incoming Reynolds number was also studied as shown in fig. IV-d. It can be clearly seen that the variation in C_l is minimal. At lower angles of attack (from 0° to 5°), the increase in Re results in a slight decrease in the C_l values which is since an increase in the Re results in a decrease in the bubble length and consequently the length of the plateau region on the C_p profile is shortened. However, at higher angles, the bubble is almost near the leading edge and hence lies within the suction peak region.

Variation of drag coeffici.ent C_d[1] with angle of attack at Reynolds number - Drag force is the friction force acting at the surface of the body moving through fluid, drag force always acts in the opposite direction of movement, because of its opposing nature it retards the motion of the body. To move the at the same speed power required will be more.

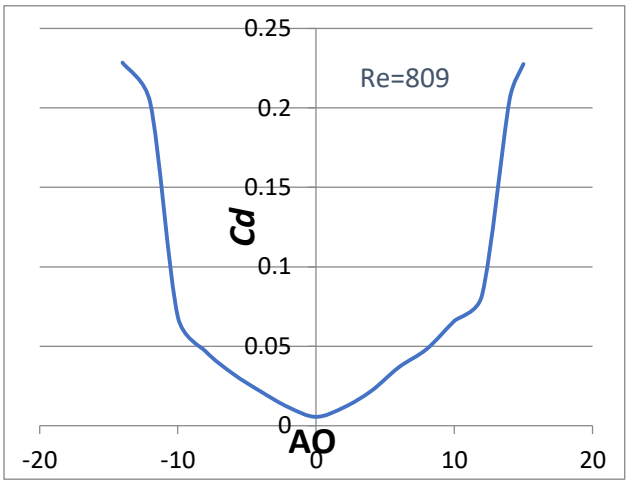

Fig. IV-e C_d versusα distribution graph

Drag Polar($C_d$versus C_l) - The Drag Polar is the relationship between the lift on an aircraft and its drag, expressed in terms of the dependence of the lift coefficient on the drag coefficient.

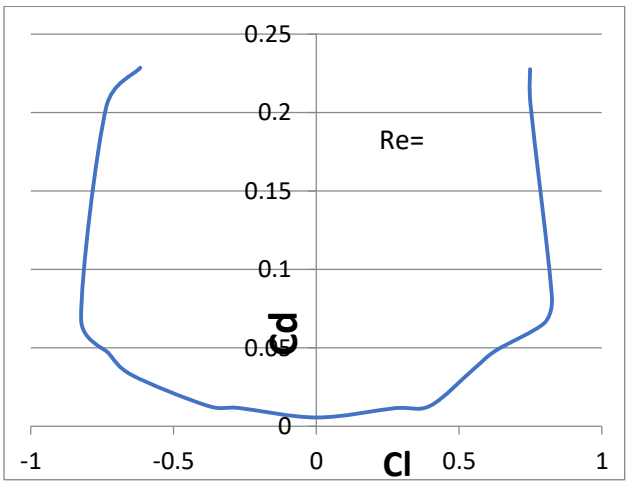

Fig. IV-f $C_d$versus $C_l$variation graph

V. CONCLUSION AND FUTURE WORK SCOPE

An experimental technique to study the characteristic of an airfoil NACA0012 was successfully implemented at fluid machinery lab. Method used to study the behavior of the Airfoil was flow of air stream at the surface of the airfoil by the help of axial fan in the wind tunnel, which provides the controlled environment to perform the experiment, to generate the pressure difference across the upper and lower surface.

Results obtained from the study Airfoil characteristics was satisfactorily matched with the standard data.

Results obtained from the study are given below

A. In this experiment a NACA 0012 airfoil was tested at 4 different velocities with a varying

angle of attack from +15° to -14°, the major results are that the coefficient of lift that the lab group determined from the symmetric airfoil data maxed at an angle of attack of 12 degrees. According to the experiment, as well as theory, the stall angle for the airfoil should be at 12 degrees.

B. In the range of angle of attack from the -12 to +12 coefficients of drag variation is very small which shows that there is small power variation to run the machine.

C. After the stall angle, which is 12° coefficient of drag varies sharply and coefficient of lift decreases which shows that more power requirement to run the machine with very small rise.

D. In the range of angle of attack -12 to +12 coefficient of lift is high but after the stall angle it start decreasing.

E. With the help of Cp variation graph, we can visualize the pressure variation along the surface of the Airfoil.

VI. REFERENCES

[1] Y. Lian, and W. Shyy, "Laminar-Turbulent Transition of a Low Reynolds Number Rigid or Flexible Airfoil", AIAA Journal, Vol. 47, No. 7, 2007.

[2] George Philip, "An experimental study on the characteristics laminar separation on the surface"

[3]http://www.mhaerotools.de/airfoils/methods.hm
http://www.wikipedia.com

[5] N Gregory, and C L O'reilly, "Low speed characteristics of NACA 0012 Airfoil Section including the effects of Upper Surface Roughness Simulating Hoar Frost" report by Ministry of Defense.

[6] Charles Holicker, "Characteristics of NACA 0012 Wing: Determination of Cl and Cd using foce Balance"

[7] Mohsen Jahanmiri, "Laminar Separation Bubble: Its Structure, Dynamics and Control", research report 2011/06

[8] http://www.aerolab.com

APPENDIX

A. coefficient of pressure at velocity of 9.82m/s

RUN NO.	1	2	3	4	5	6	7	8	9	10	11	12	13	14	15	16
AOA	-14	-12	-10	-8	-6	-4	-2	0	2	4	6	8	10	12	14	15
P0	30	29	28	27	26	26	26	25	24	24	23	22	21	21	21	20
Pinf	38	37	35	35	34	34	34	33	31	32	31	30	30	29	29	28
LE	45	45	56	50	42	34	29	25	24	24	24	27	30	30	24	24
U1	31	30	39	28	29	30	31	35	37	40	42	42	48	52	36	35
U2	33	32	31	31	31	32	33	36	37	38	40	40	46	48	36	35
U3	35	34	32	32	33	34	35	36	37	38	39	41	41	40	36	35
U4	36	35	33	33	33	35	35	36	37	37	38	40	39	38	35	35
U5	37	35	34	34	34	35	35	36	37	37	37	39	38	37	35	34
U6	37	35	34	34	34	35	35	36	36	36	36	37	37	36	34	34
U7	37	35	34	34	34	34	34	35	35	35	36	35	35	35	34	34
U8	38	36	35	35	35	35	35	36	35	35	36	35	35	34	34	34
U9	37	36	35	34	34	34	34	35	34	35	36	34	33	32	33	33
U10	37	35	34	34	34	33	33	35	34	34	32	32	32	31	33	33
U11	37	35	35	34	34	33	33	34	33	33	32	32	31	30	33	32
U12	38	36	35	34	34	33	33	34	33	32	31	31	31	30	33	32
U13	38	36	35	34	34	33	33	33	33	32	31	31	30	29	32	32
U14	38	36	35	34	34	33	32	33	33	31	31	30	30	29	32	32
U15	39	36	35	34	33	33	32	33	32	30	30	29	29	28	31	31
TE	38	35	34	33	32	32	31	32	31	29	29	28	28	27	29	29
LE	45	45	56	50	42	34	29	25	24	24	24	27	30	30	24	24
L1	42	43	51	49	45	41	38	34	31	28	26	24	22	21	21	21
L2	43	44	50	47	43	40	38	35	32	30	28	26	25	23	24	23
L3	42	43	45	45	41	39	37	35	32	30	28	27	25	24	24	24
L4	43	43	42	42	41	39	37	35	33	31	29	28	26	25	25	25
L5	43	43	41	41	40	38	37	35	33	31	30	29	27	26	27	26
L6	43	43	40	40	39	38	36	35	33	32	30	29	28	27	27	27
L7	43	42	40	39	38	37	36	35	33	32	30	30	28	27	28	27
L8	43	41	49	38	37	36	35	33	32	31	30	29	28	27	27	27
L9	43	40	38	36	36	35	35	32	32	31	29	29	28	27	27	27
L10	43	40	37	36	35	34	35	32	31	30	29	29	28	27	27	27
L11	42	40	36	36	35	34	34	32	31	30	30	29	28	28	28	28
L12	42	40	36	35	35	34	34	32	31	30	30	29	28	28	29	28
TE	38	35	34	33	32	32	31	32	31	29	29	28	28	27	29	29

B. Data Acquisition Sheet at 8.5m/s

RUN NO.	1	2	3	4	5	6	7	8	9	10	11	12	13	14	15	16	17
AOA	-14	-12	-10	-8	-6	-4	-2	0	2	4	6	8	10	12	14	15	6
P0	30	29	28	27	26	26	26	25	24	24	23	22	21	21	21	20	20
Pinf	38	37	35	35	34	34	34	33	31	32	31	30	30	29	29	28	28
LE	78	79	87	81	76	72	68	65	64	65	64	66	68	69	65	64	65
U1	68	67	66	67	67	68	70	72	74	77	78	80	82	84	74	73	79
U2	69	68	67	68	69	70	70	72	74	75	76	77	80	83	73	72	76
U3	70	69	69	69	70	70	71	73	74	75	75	76	79	77	73	72	75
U4	71	70	70	70	71	71	72	73	74	75	75	76	76	75	73	72	75
U5	70	70	69	69	70	70	71	72	73	73	73	74	74	73	71	71	73
U6	71	71	70	70	71	71	72	72	73	74	73	74	74	73	72	72	73
U7	71	70	70	70	70	71	71	72	72	73	73	72	72	72	72	71	72
U8	72	71	71	71	71	71	72	72	73	73	73	72	72	72	73	72	72
U9	72	71	70	70	70	71	71	71	72	72	72	71	71	70	72	71	70
U10	71	70	70	70	70	70	70	70	71	72	70	70	70	69	71	71	69
U11	72	71	70	70	70	70	70	70	71	71	70	70	70	69	71	71	69
U12	72	71	70	70	70	70	70	71	71	71	70	69	69	69	72	71	69
U13	72	71	70	70	70	70	70	70	70	70	69	69	69	68	71	71	68
U14	73	71	70	70	70	70	70	70	70	70	69	69	69	68	71	71	68
U15	73	71	70	70	70	70	70	70	69	70	68	68	68	68	70	70	67
TE	73	71	70	69	70	70	69	69	68	69	67	67	67	67	69	69	66
LE	78	79	87	81	76	72	68	65	64	65	64	66	68	69	65	64	65
L1	76	77	83	80	78	76	74	71	69	68	65	64	63	63	63	63	63
L2	76	78	83	79	77	76	74	72	70	69	67	66	65	64	65	64	65
L3	75	77	80	77	76	74	73	71	70	69	67	66	65	65	65	65	65
L4	76	77	77	76	76	74	73	72	70	70	68	67	66	66	66	66	66
L5	76	77	76	75	76	74	73	72	71	70	69	68	67	67	67	67	67
L6	76	77	75	75	75	74	73	72	71	71	69	68	68	67	68	67	67
L7	76	76	74	74	74	73	73	72	71	70	69	68	68	68	68	67	67
L8	75	75	73	73	73	72	72	71	70	70	68	68	67	67	67	67	67
L9	75	74	72	72	72	71	71	70	69	69	68	67	67	67	67	67	66
L10	74	74	71	71	72	71	71	70	69	69	68	67	67	67	67	67	66
L11	75	74	71	71	72	71	71	70	69	69	68	68	68	67	68	67	67
L12	75	74	71	71	71	71	71	70	69	69	68	68	68	67	68	68	67
TE	73	71	70	69	70	70	69	69	68	69	67	67	67	67	69	69	66

C. Data Acquisition Sheet at 7.76m/s

RUN NO.	1	2	3	4	5	6	7	8	9	10	11	12	13	14	15	16	17
AOA	-14	-12	-10	-8	-6	-4	-2	0	2	4	6	8	10	12	14	15	6
P0	30	29	28	27	26	26	26	25	24	24	23	22	21	21	21	20	20
Pinf	38	37	35	35	34	34	34	33	31	32	31	30	30	29	29	28	28
LE	67	68	72	70	66	63	60	45	45	45	46	47	48	46	46	45	44
U1	60	60	59	59	60	61	62	52	53	55	57	58	60	54	52	51	54
U2	61	61	60	60	61	62	63	52	53	54	55	56	58	54	52	51	52
U3	62	62	61	61	62	63	63	52	53	54	54	56	55	53	52	51	52
U4	62	63	61	62	62	64	64	53	53	54	54	55	53	53	52	51	52
U5	62	62	61	61	61	63	63	52	52	53	53	54	53	52	51	50	51
U6	63	63	62	62	62	63	64	52	52	53	53	54	52	52	52	51	51
U7	63	63	61	62	62	63	63	51	52	52	53	52	52	51	51	50	51
U8	64	63	62	63	63	63	64	52	52	53	53	52	52	52	52	51	51
U9	63	63	62	62	62	63	63	51	51	51	52	51	51	51	51	50	50
U10	63	63	61	61	61	62	62	50	50	51	50	50	50	50	51	49	49
U11	63	63	61	61	61	62	62	50	50	51	50	50	49	50	51	50	48
U12	63	63	61	62	61	62	62	50	50	50	50	50	49	50	51	50	48
U13	63	63	61	62	61	62	62	50	50	50	50	49	49	50	51	50	48
U14	64	63	61	62	62	62	62	50	50	50	49	49	49	50	51	50	48
U15	64	63	61	61	62	62	62	49	49	49	48	49	48	49	50	49	47
TE	63	63	61	61	61	61	61	48	48	48	48	48	47	48	49	48	46
L1	65	67	70	70	68	67	65	50	49	47	46	45	44	44	45	43	44
L2	66	67	70	69	67	66	65	50	50	49	47	47	45	46	46	45	46
L3	65	66	68	68	66	65	64	50	49	49	47	47	46	46	46	45	46
L4	66	67	67	68	66	66	65	51	50	49	48	48	47	47	47	46	47
L5	66	67	66	66	66	65	65	51	50	50	49	49	48	48	48	47	47
L6	66	67	66	66	65	65	65	51	50	50	49	49	48	48	48	47	48
L7	66	66	65	65	65	65	65	51	50	50	49	49	48	48	49	47	48
L8	65	65	64	64	64	64	64	50	49	49	49	48	47	48	48	47	47
L9	65	65	63	63	63	63	63	49	49	49	48	48	47	48	47	46	46
L10	65	64	63	63	62	63	63	49	49	49	48	48	47	48	47	47	46
L11	65	64	63	63	62	63	63	49	49	49	49	48	48	48	48	47	47
L12	65	64	63	63	62	63	63	50	49	49	49	48	48	48	48	47	47
TE	73	71	70	69	70	70	69	69	68	69	67	67	67	67	69	69	66